INORGANIC CHEMISTRY
FRONTIERS

RESEARCH ARTICLE

View Article Online
View Journal | View Issue

Cite this: *Inorg. Chem. Front.*, 2024, **11**, 7898

Tuning the phototherapeutic activity of Pt(IV) complexes for bladder cancer *via* modification of *trans N*-heterocyclic ligands†

Huayun Shi, * Guy J. Clarkson and Peter J. Sadler *

Bladder cancer is a common cancer globally that suffers from expensive treatment, drug and hypoxia resistance, and high recurrence rate. A series of six novel diazido Pt(IV) complexes with the general formula *trans*, *trans*, *trans*-$[Pt(N_3)_2(OH)_2(L)_2]$ and various equatorial *N*-heterocyclic amine ligands (L = pyridines: **1** and **3–6**; or imidazole: **2**) have been synthesised and characterised, including their X-ray crystal structures, and their photoactivation investigated. The L-substituents modify the photocytotoxicity of these complexes towards bladder cancer cells significantly. In general, strong electron-withdrawing substituents result in higher photocytotoxicity compared to unsubstituted *trans*, *trans*, *trans*-$[Pt(N_3)_2(OH)_2(py)_2]$ (**FM190**) and enhanced photocytotoxicity under hypoxia than normoxia, but higher dark cytotoxicity as well. Among them, the nitroimidazole complex **2**, *trans*, *trans*, *trans*-$[Pt(N_3)_2(OH)_2$(1-methyl-5-nitroimidazole)$_2]$, exhibits low dark cytotoxicity and promising photocytotoxicity with blue-light irradiation IC_{50} values < 5 μM towards a series of bladder cancer cell lines under both normoxia and hypoxia. Notably, its green-light photocytotoxicity was significantly enhanced (>15×) under hypoxia compared to normoxia. Low cytotoxicity (IC_{50} 14.4–100 μM) was observed towards normal bladder cells, even upon irradiation. Although photoinduced ROS generation, apoptosis and lipid peroxidation were observed for **2** under normoxia rather than hypoxia, high nuclear Pt accumulation, increased photoactivation in the medium, significantly enhanced cellular Pt accumulation and mitochondrial membrane potential changes upon irradiation under hypoxia were observed. These results suggest different mechanisms of action for **2** under normoxia and hypoxia. In addition, **2** exhibited high liver microsomal dark stability and photo-enhanced Pt accumulation in rat bladder. Based on these results, complex **2** is a promising candidate for phototherapeutic bladder cancer treatment.

Received 13th July 2024,
Accepted 26th August 2024

DOI: 10.1039/d4qi01765j

rsc.li/frontiers-inorganic

10th anniversary statement

We have been pleased to publish some of our exciting interdisciplinary medicinal inorganic chemistry discoveries on the design and novel mechanisms of action of metal coordination anticancer complexes in Inorganic Chemistry Frontiers.

Our publications have included catalytic half-sandwich organometallic iridium anticancer complexes which can modulate redox pathways in cells utilizing coenzyme nicotinamide adenine dinucleotide (https://doi.org/10.1039/C4QI00098F), nanoparticles of natural polymers conjugated to organometallic complexes as drug delivery systems (https://doi.org/10.1039/C6QI00115G), and direct studies of in-cell activation of inert osmium complexes using synchrotron nanoprobe X-ray fluorescence (https://doi.org/10.1039/D1QI00512J).

Our research on photactivatable multifunctional platinum prodrugs for cancer chemotherapy (https://doi.org/10.1039/C9QI00288J; https://doi.org/10.1039/d0qi00685h) has progressed to the discovery of induced immunogenic cancer cell death (https://doi.org/10.1039/D0QI00991A), and now complexes which are highly active under hypoxia and promising candidates for phototherapeutic bladder cancer treatment (https://doi.org/10.1039/d4qi01765j).

ICF is a showcase for innovative interdisciplinary inorganic chemistry and I have been fortunate to publish with talented international coauthors, including those from China, Spain, Italy, Czechia, France, Venezuela and the UK.

Introduction

Phototherapy provides cancer selectivity by using spatially and temporally controllable light with minimal invasiveness.[1–3] Different from current clinically used photodynamic therapy (PDT) agents based on an oxygen-dependent mechanism,

Department of Chemistry, University of Warwick, Coventry CV4 7AL, UK.
E-mail: Huayun.shi@warwick.ac.uk, p.j.sadler@warwick.ac.uk

† Electronic supplementary information (ESI) available. CCDC 2359629, 2359630, 2360200, 2360222, 2360223 and 2360225. For ESI and crystallographic data in CIF or other electronic format see DOI: https://doi.org/10.1039/d4qi01765j

photoactive diazido Pt(IV) complexes have been developed as a new generation of photoactivated chemotherapy (PACT) anticancer agents, which remain stable in the dark and exert photocytotoxicity independent from oxygen.[4–6] Hypoxia, a hallmark of the tumour microenvironment, results from the rapid proliferation of tumours and blood vessel deformation, alters cancer cell metabolism, and contributes to therapy resistance, including chemotherapy, radiotherapy and PDT.[7,8]

Bladder cancer (BC) is recognised as the most expensive tumour due to its high recurrence rates, intensive surveillance strategies, and expensive treatment costs.[9–11] Cisplatin is a standard chemotherapeutic agent used for BC, but limited by its low response rate and high resistance incidence.[12–14] Phototherapy is attractive for BC treatment due to the ease of light accessibility for the bladder cavity *via* an endoscope.[15–19] Photofrin, the first PDT agent, was approved to treat BC with red light (630 nm) in 1993 in Canada, but abandoned due to skin photosensitivity and compromised bladder function caused by the deep tissue penetration of red light.[1,20,21] In contrast, green light (525 nm) is used to activate TLD1433 for NMIBC to reduce PDT-induced damage to the bladder wall.[18] Successful phase II results have been obtained for TLD1433, but as a PDT agent, its oxygen-dependent mechanism results in its significantly reduced photocytotoxicity under hypoxia.[18] Increased angiogenesis in BC indicates tissue hypoxia and is associated with a low survival rate.[17,22]

Photoactive diazido Pt(IV) complexes with oxygen-independent mechanisms have potential as new phototherapeutic agents for BC.[4] However, killing bladder cancer cells is very challenging. The photo IC_{50} values for a series of diazido Pt(IV) complexes, including *trans*, *trans*, *trans*-$[Pt(N_3)_2(OH)_2(py)(NH_3)]$, towards the 5637 human bladder cancer cell line have been reported to be >30 μM with UVA irradiation.[23,24] *Trans*, *trans*, *trans*-$[Pt(N_3)_2(OH)_2(py)_2]$ (**FM190**), a promising current lead compound, shows no apparent photocytotoxicity with blue light towards SW780 bladder cancer cells with a short incubation time (1 h incubation, 1 h irradiation and 24 h recovery), but is active when conjugated to ferrocene through a flexible bridging ligand.[25,26] It is important now to study especially the photocytotoxicity of these complexes towards bladder cancer cells under hypoxia.

Although axial functionalisation is the most common strategy for the optimisation of anticancer Pt(IV) complexes, the nature of the equatorial ligands can also alter the photoactivation and photocytotoxicity of diazido Pt(IV) complexes.[27] *Trans*, *trans*, *trans*-$[Pt(N_3)_2(OH)_2(NH_3)(py)]$ kills cancer cells in the presence of UVA irradiation (365 nm),[28] while the bis-pyridine complex **FM190** shows photocytotoxicity with blue light (420 nm).[25] Introduction of methyl substituents can alter the UV-vis absorption, photoactivation and photocytotoxicity of **FM190**.[27] The nitro group is a strong electron-withdrawing substituent used in a wide variety of bioactive molecules[29] and can red-shift the absorption spectra of diazido Pt(IV) complexes as a substituent on equatorial pyridines.[30]

Nitroimidazole antibiotics, such as metronidazole and tinidazole, are approved drugs for treatment of anaerobic bacterial and parasitic infections.[31,32] Hypoxia is essential for these nitroimidazole antibiotics to exert their effects, since reduction of the nitro group generates toxic intermediates that can bind to DNA covalently.[33] The presence of oxygen can inhibit or reverse reduction of nitroimidazoles.[32] The anticancer and antimicrobial ability of nitroimidazole derivatives has also been investigated, especially when they are coordinated to metal complexes.[34–36] Pt(II)-nitroimidazole complexes have been developed as radiosensitisers for anticancer radiotherapy under hypoxia.[37–40] Compared with traditional Pt drugs, such as cisplatin, these complexes exhibit higher cytotoxicity under hypoxia than normoxia due to the reduction of the nitroimidazole.

Here we report a series of six new photoactive diazido Pt(IV) complex with the general formula, *trans*, *trans*, *trans*-$[Pt(N_3)_2(OH)_2(L)_2]$ (L = pyridines: **1** and **3–6**; or imidazole: **2**), and for which all of their structures were characterised by X-ray crystallographic analysis. Based on the photoactivation with visible light and cytotoxicity studies, nitroimidazole complex **2**, *trans*, *trans*, *trans*-$[Pt(N_3)_2(OH)_2$(1-methyl-5-nitroimidazole)$_2]$, was selected as the lead complex for further investigation due to its promising photocytotoxicity towards series of bladder cancer cell lines under both normoxia and hypoxia. Its redox behaviour, dark stability and photoactivation in the presence of GSH, photoreaction with guanosine 5′-monophosphate (5′-GMP), and photocytotoxicity under various oxygen concentrations were investigated. The Pt cellular accumulation and distribution, generation of ROS, mitochondrial membrane potential change and mechanisms of action of **2** were determined under various oxygen concentrations. In addition, its liver microsomal dark stability and the Pt accumulation in rat bladder were also explored. Our findings suggest that the introduction of nitroimidazole ligands can improve the photocytotoxicity of diazido Pt(IV) complexes, especially under hypoxia, overcome cisplatin and hypoxia resistance, and provide a basis for a promising phototherapeutic Pt drug candidate for treatment of BC.

Results

Synthesis and characterisation

Six photoactive diazido Pt(IV) with varied *N*-heterocyclic amine ligands were synthesised and characterised (Fig. 1a). The synthetic route is summarised in Scheme S1.† The complexes were obtained by oxidation of *trans*-diazido Pt(II) complexes containing the corresponding *N*-heterocyclic amine ligands using H_2O_2. They were characterised by HPLC (Fig. S1†) with purity higher than 99%, ESI-HR-MS (Fig. S2†), NMR (Fig. S3–14†) and UV-vis spectra (Fig. 1b).

The ^1H and ^{13}C NMR spectra are consistent with the proposed structures (Fig. S3–14†). All complexes show ^1H NMR signals with ^{195}Pt satellites. Among them, complexes containing pyridine ligands with *meta* electron-withdrawing substituents, **1** and **3**, have a ^1H NMR singlet and a doublet with ^{195}Pt satellites assignable to the *ortho* protons on pyridine. The

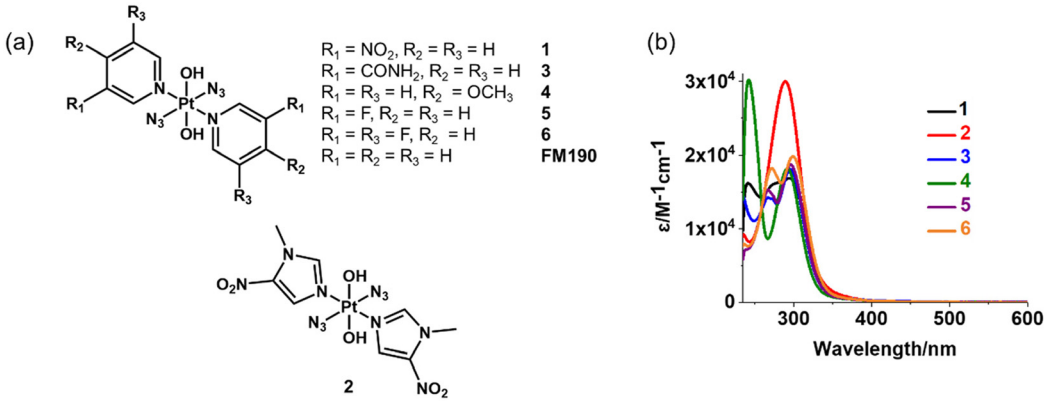

Fig. 1 (a) Structures of photoactive diazido Pt(IV) complexes **1–6** (*trans, trans, trans*-$[Pt(N_3)_2(OH)_2(L)_2]$, L = 3-nitropyridine **1**, 1-methyl-5-nitroimidazole **2**, nicotinamide **3**, 4-methoxypyridine **4**, 3-fluoropyridine **5**, and 3,5-difluoropyridine **6**), and parent complex **FM190**; (b) UV-vis spectra of complexes **1–6** in water at 298 K.

strong electron-withdrawing nitro group in **1** results in the low-field shifts to 9.92 and 9.40 ppm for these *ortho* protons. Complex **4** with symmetric pyridine ligands shows one doublet with ^{195}Pt satellites and another doublet for *ortho* and *meta* protons, respectively. The presence of F (nuclear spin I = 1/2) induces more complicated splitting of ^{1}H and ^{13}C NMR signals for complexes **5** and **6**. The *ortho* protons on **5** gave one triplet and one doublet with Pt satellites due to the coupling with ^{19}F and ^{1}H, respectively. While symmetric **6** show a triplet with Pt satellites for *ortho* protons. The ^{1}H NMR spectrum of **2** shows two singlets with ^{195}Pt satellites at 9.0 and 9.50 ppm assignable to protons on the imidazole ring. Two singlets at 4.17 and 1.61 ppm from CH_3 and OH, respectively, are also detectable for **2**.

Complexes with pyridine derivatives exhibit similar absorption spectra despite the effect of the substituents, usually an absorption maximum at *ca.* 295 nm and a peak at 240–270 nm with a moderate extinction coefficient of *ca.* 15 000 M^{-1} cm^{-1} in water (Table S1† and Fig. 1b). In addition, a shoulder at 275 nm was observed for **1** due to the presence of the nitro group. The only exception is **4** with a methoxy substituent, which contains a peak at 242 nm with a high extinction coefficient of 30 167 M^{-1} cm^{-1}. In contrast, a peak maximum at 289 nm (ε = 30 007 M^{-1} cm^{-1}) was detected for **2** (L = 1-methyl-5-nitroimidazole).

Crystal structures

Crystals suitable for X-ray diffraction were obtained through the evaporation of methanol solutions of the complexes. A perspective drawing of complexes **1–6** is shown in Fig. 2. The crystallographic data are summarised in Tables S2 and S3,† and selected bond distances and angles are listed in Tables S4 and S5.† Complexes **1**, **2** and **4** crystallised in monoclinic space groups $P2_1/c$ (**1**), $C2/c$ (**2**) and $P2_1/n$ (**4**), respectively, while complexes **3**, **5** and **6** crystallised in the monoclinic space group P-1.

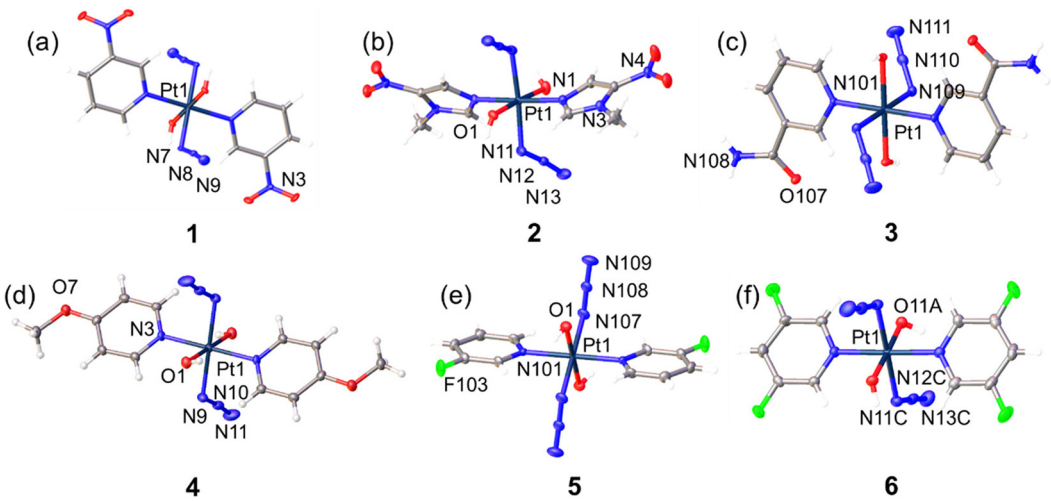

Fig. 2 Crystal structures of complexes *trans, trans, trans*-$[Pt(N_3)_2(OH)_2(L)_2]$ (L = 3-nitropyridine **1**, 1-methyl-5-nitroimidazole **2**, nicotinamide **3**, 4-methoxypyridine **4**, 3-fluoropyridine **5**, and 3,5-difluoropyridine **6**). Only the heteroatoms of the asymmetric unit are labelled and thermal ellipsoids are drawn at 50% probability level.

The octahedral platinum centre of these complexes with an $[N_4O_2]$ geometry is similar to **FM190**, with an all-*trans* configuration of the coordinated ligands. Platinum in **1**, **3**, **4**, **5** and **6** sits on a crystallographic inversion centre, and the two pyridine rings bound to the Pt are parallel to each other. In contrast, the two *trans* imidazole ligands in **2** are not in the same plane. The angle between mean planes through two imidazole ligands in one molecule is 61.764 (0.101)°. Many of the electron-donating or electron-withdrawing substituents are involved in the formation of hydrogen bonds in the solid state (Table S6†). Generally, hydrogen bonds observed in these crystal structures are moderately strong with donor–acceptor distances, d(D–A), in the range of 2.6–3.5 Å. Hydrogen bonds between strong hydrogen donors and acceptors, such as axial Pt–O–H, $C(O)NH_2$, H_2O and CH_3OH molecules from solvent residue, are strong with donor–acceptor distances < 2.9 Å, while close contacts involving the N_3 ligands, F atoms, or even C–H are relatively weak with donor–acceptor distances > 2.9 Å. Notably, the hydrogen bonds involve $C(O)NH_2$, O2–H2···O107 and N108–H10A···O2 between axial Pt–O–H and $C(O)NH_2$ and that between $C(O)NH_2$ and N_3 ligand N108–H10B···N109 can be found in **3**.

Photoactivation in aqueous solution

Photoactivation upon irradiation with blue (463 nm) or green (517 nm) light for Pt(IV) complexes **1–6** in air- or N_2-saturated aqueous solution at 298 K was monitored by UV-vis spectroscopy (Fig. 3 and S15–S17†). A significant decrease in absorbance at *ca.* 290 nm (LMCT band) was observed for all complexes when exposed to blue light, which was rapid during the first 40 min, then reached a plateau afterwards (Fig. 3a, b and S16a–d†). In contrast, the decrease in LMCT band occurs more slowly with green light (Fig. 3c, d and S16e–h†). Complexes in N_2-saturated solution exhibited a similar photoactivation rate compared with the air-saturated solution upon light exposure (Fig. S15 and S17†).

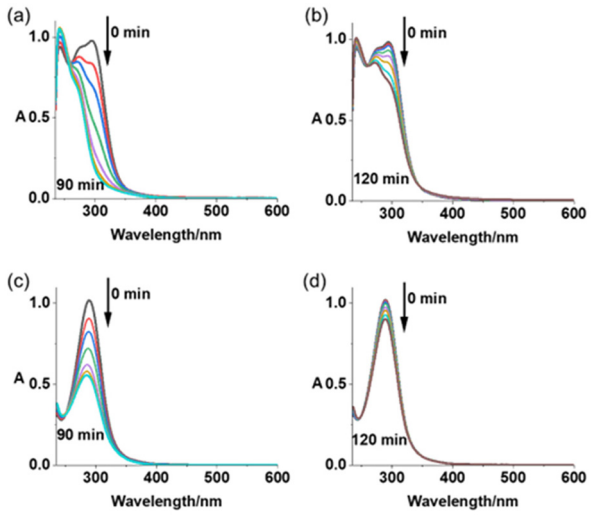

Fig. 3 UV-vis spectral changes for complexes **1** and **2** in air-saturated water exposed to blue (463 nm, a for **1**; c for **2**) or green (517 nm, b for **1**; d for **2**) light at 298 K, recorded after 0, 5, 10, 20, 40, 60, 90 and 120 min irradiation.

To explore the photoproducts from these complexes, LC-MS was used to monitor the photoactivation reactions in aqueous solution. Complexes **1** and **2** display extremely high dark stability at 310 K in aqueous solution (Fig. S18a and c†). In contrast, 1 h irradiation with blue light (463 nm) resulted in photoactivation of 97% of **1** and 95% of **2** (Tables S7 and S8, Fig. S18b and d†). For **1**, the main Pt-containing photoproducts are assigned as $[2\{Pt^{IV}(\mathbf{L1})_2(N_3)(OH)_3\} + H]^+$(*m*/*z* 1072.91), $\{Pt^{II}(\mathbf{L1})_2(N_3)(CH_3CN)\}^+$ (*m*/*z* 525.93), and $\{Pt^{III}(\mathbf{L1})_2(HCOO)_2\}^+$ (*m*/*z* 532.93), while for **2**, $[2\{Pt^{IV}(\mathbf{L2})_2(N_3)(OH)_3\} + H]^+$ (*m*/*z* 1084.95), $\{Pt^{IV}(\mathbf{L2})_2(m/z\ HCOO)_3\}^+$ (583.99), $\{Pt^{II}(\mathbf{L2})_2(N_3)(CH_3CN)\}^+$ (*m*/*z* 531.97), and $\{Pt^{II}(\mathbf{L2})_3(N_3)\}^+$ (*m*/*z* 618.08). Notably, released **L1** ligand (3-nitropyridine + H^+, *m*/*z* 124.97) was detectable in photoactivated solutions of **1**. CH_3CN and $HCOO^-$ ligands arise from the mobile phase. Green light (517 nm) also induces photoactivation of both compounds, but the proportion of activated molecules and number of Pt photoproducts are lower compared with blue light, with the ratio being 14% and 16% for **1** and **2**, respectively. Pt species $\{Pt^{III}(\mathbf{L1})_2(OH)_2\}^+$ (*m*/*z* 476.89) and $\{Pt^{II}(\mathbf{L1})_2(N_3)(CH_3CN)\}^+$ (*m*/*z* 525.93) are assigned as the main photoproducts for **1**, whilst they are $\{Pt^{III}(\mathbf{L2})_2(OH)_2\}^+$ (*m*/*z* 482.92), $\{Pt^{II}(\mathbf{L2})_2(N_3)(CH_3CN)\}^+$ (*m*/*z* 531.97), and $\{Pt^{II}(\mathbf{L2})_3(N_3)\}^+$ (*m*/*z* 618.08) for **2**.

Azidyl radicals are important photocytotoxic products from Pt(IV) complexes and can be trapped by DMPO and detected using EPR. A mixture of 2.5 mM complexes (**1** or **2**) and 40 mM DMPO in MilliQ water was irradiated continuously by blue light (463 nm) and monitored by EPR (Fig. S19†). The azidyl radical adduct DMPO-$N_3^{\bullet}$ was detected as a 1 : 2 : 2 : 1 quartet of triplets with parameters in good agreement with previously reported data.[41] The generation of singlet oxygen was determined in the mixture of 2.5 mM complexes (**1** or **2**) and 20 mM TEMP in acetonitrile with continuous blue light (463 nm) irradiation using EPR (Fig. S20†). The 1 : 1 : 1 triplet of singlet indicates the formation of TEMPO, the oxidation product of TEMP by singlet oxygen.

Photocytotoxicity

The photocytotoxicity of **1–6** under normoxic (21% O_2) and hypoxic (1% O_2) environments towards SW780 human bladder cancer cell line was investigated upon irradiation with blue (465 nm) and green (520 nm) light in comparison with parent complex **FM190** and cisplatin (Tables S9 and S10,† Fig. 4a, S21 and S22†). The cell survival rate was determined by the sulforhodamine B (SRB) colorimetric assay after 1 h incubation, 1 h irradiation and 72 h after-treatment incubation to mimic the clinical conditions.

Complexes with strong electron-withdrawing substituents on pyridine, **1** and **6**, as well as parent compound without substituents, **FM190**, display moderate dark cytotoxicity (IC_{50} of 15.1–74.4 μM under normoxia; 14.4–82.2 μM under hypoxia) due to the long incubation time. In contrast, complexes with moderate electron-withdrawing or electron-donating substitu-

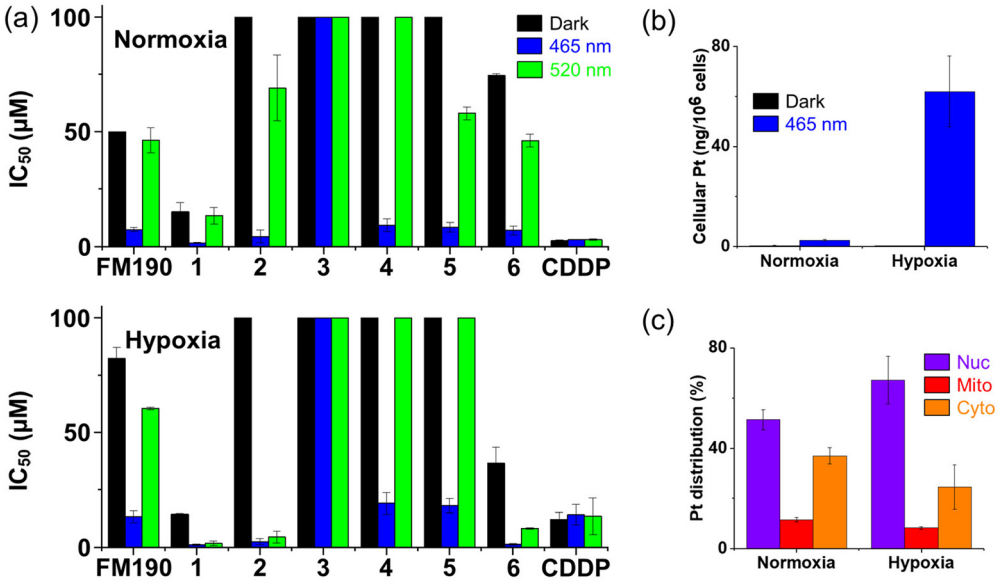

Fig. 4 (a) IC_{50} values for complexes **1–6** in SW780 bladder cancer cells after 1 h incubation, 1 h irradiation (blue 465 nm, green 520 nm) and 72 h further incubation under normoxia (21% O_2) or hypoxia (1% O_2). CDDP (cisplatin) and **FM190** were studied for comparison. Values and errors are listed in Tables S9 and S10.† (b) Cellular accumulation (ng per 10^6 cells) and (c) distribution (%) of Pt in SW780 bladder cancer cells after exposure to complex **2** (10 μM, 2 h in the dark) under normoxia or hypoxia. Nuclei (Nuc), mitochondria (Mito), and cytoplasm excluding the mitochondrial component (Cyto), were isolated by using a mitochondrial isolation kit.

ents on pyridine, **3–5**, exhibit low dark cytotoxicity with IC_{50} > 100 μM, under both normoxia and hypoxia. Notably, despite the presence of the strong electron-withdrawing nitro group, complex **2** shows low dark cytotoxicity (IC_{50} > 100 μM). Upon irradiation with blue light, the photocytotoxicity of these complexes follows the trend: **1** (1.6 μM) > **2** (4.4 μM) > **6** (7.0 μM) > **FM190** (7.4 μM) > **5** (8.4 μM) > **4** (9.3 μM) > **3** (>100 μM) under normoxia; and **1** (1.1 μM) > **6** (1.3 μM) > **2** (2.4 μM) > **FM190** (13.3 μM) > **5** (18.1 μM) > **4** (19.1 μM) > **3** (>100 μM) under hypoxia (Fig. 4a). Interestingly, only complexes with strong electron-withdrawing substituents, **1**, **2** and **6**, exhibit higher photocytotoxicity than unsubstituted **FM190**, as well as enhanced photocytotoxicity under hypoxia than normoxia with blue light. Furthermore, with green light exposure, these three complexes exhibit a significant increase in photocytotoxicity under hypoxia. In contrast, complex **3** with a $CONH_2$ group exhibits no photocytotoxicity under all conditions. For comparison, the cytotoxicity of cisplatin is not affected by irradiation, but reduced when the oxygen concentration decreases.

Based on the promising photocytotoxicity and low dark cytotoxicity of **2** towards SW780 cells under all conditions, it was selected as the lead complex for further exploration. Complex **1** was used for comparison due to the presence of a nitro group and its high photocytotoxicity. Their photocytotoxicity towards a series of human cell lines, including VM-CUB-1 bladder, A2780 and cisplatin resistant A2780cis ovarian cancer cells, SV-HUC-1 normal bladder epithelial cells and MRC-5 lung fibroblast was investigated upon irradiation with blue (465 nm) and green light (520 nm) in comparison with parent complex **FM190** and cisplatin (Tables S9, S11 and Fig. S23†).

Complex **2** exhibits no apparent dark cytotoxicity (IC_{50} > 100 μM) towards all cell lines under both normoxia and hypoxia (Tables S9 and S11†). In contrast, moderate dark cytotoxicity was determined for **1** (IC_{50} of 3.4–19.2 μM) under normoxia. The dark IC_{50} values for **1** are in general higher under hypoxia (8.6–14.8 μM) than normoxia, suggesting lower dark cytotoxicity under hypoxia.

With blue light irradiation, both complexes exhibit single-digit μM photo IC_{50} values (1.0–3.6 μM for **1**; 1.7–3.7 μM for **2**) towards cancer cells under both normoxia and hypoxia (Tables S9 and S11†). Green light with longer wavelength and deeper tissue penetration is more clinically relevant than blue light.[1] Complex **2** exhibits photocytotoxicity indices (PIs) of 1.3–7.3 upon green light irradiation under normoxia, while **1** and **FM190** show no apparent enhanced potency with green light under normoxia. Enhanced green light photocytotoxicity was observed under hypoxia, especially **1** with all IC_{50} values of *ca.* 1 μM, indicating an ability to overcome resistance induced by hypoxia. Notably, no apparent difference in photo IC_{50} values towards A2780 and resistant A2780cis cell lines indicates the ability of these complexes to overcome cisplatin resistance. In contrast, a *ca.* 10× decrease in potency was observed for cisplatin towards A2780cis compared with wild type A2780. In addition, cisplatin displayed *ca.* 1.5–12× decrease in photocytotoxicity under hypoxia compared with normoxia. For comparison, parent complex **FM190** exhibited higher dark cytotoxicity and lower photocytotoxicity towards bladder cancer cell lines than **2**, and lower photocytotoxicity under hypoxia than normoxia.

Low blue-light photocytotoxicity towards normal MRC-5 lung fibroblast (8.9 μM) and SV-HUC-1 normal bladder epi-

thelial cells (14.4 μM) was observed for **2**, indicating its good selectivity *versus* cancer cells (3.3× for SW780 and 5.8× for VM-CUB-1 against SV-HUC-1 under normoxia, Tables S9 and S11†). No enhanced cytotoxicity was observed for **1** towards SV-HUC-1 cells after irradiation. Notably, both complexes exhibit no apparent cytotoxicity towards SV-HUC-1 cells with green light irradiation. In contrast, cisplatin exhibits similar or lower (up to 7×) cytotoxicity towards cancer cells compared with MRC-5 and SV-HUC-1 cells.

Electrochemistry

The cyclic voltammograms of complexes **1** and **2**, and corresponding nitro-substituted ligands (1 mM) in acetonitrile were acquired at 298 K, using 0.1 M NBu_4PF_6 as supporting electrolyte (Table S12 and Fig. S24†). A reversible reduction wave was observed for nitro-substituted ligands due to the reduction of the nitro group, assignable to Ar-NO_2/Ar-$NO_2^{\bullet-}$ (ligand: **L1**: E_{pa}: −1.29 V; E_{pc}: −1.38 V; **L2**: E_{pa}: −1.454 V; E_{pc}: −1.547 V). For Pt complexes, the reversible reduction of the nitro group is similar to the ligands alone (**1**: E_{pa}: −1.28 V; E_{pc}: −1.367 V; **2**: E_{pa}: −1.308 V; E_{pc}: −1.376 V). An irreversible reduction wave assigned to Pt^{IV}/Pt^{II} was also determined as −0.974 V for **1**; −1.208 or −1.506 V for **2**; −1.38 V for **FM190**, which correlated with the dark stability: **2** > **FM190** > **1**.

Dark stability and photoreactions with biomolecules

No apparent UV-vis spectral change was observed for air- or N_2-saturated PBS solution containing Pt(IV) complexes **1** or **2** in the presence of 2 mM GSH in the dark at 298 K for 2 h, suggesting promising dark stability towards bioreductants (Fig. S25a, 25d, S26a and 26d†). Their dark stability in the presence of 2 mM GSH was also monitored by LC-MS, with about 79% and 68% of **1** and **2**, respectively, remaining after 24 h incubation at 310 K in the dark (Fig. S27†).

In contrast, upon irradiation of blue (463 nm) light, an apparent decrease in the absorbance at *ca.* 290 nm (LMCT band) was detected for the same solutions at a similar rate as for the complex alone (Fig. S25b and e†). N_2-saturated solutions exhibited a relatively faster decomposition rate compared with air-saturated solutions, especially upon green light exposure (Fig. S26b–f†). The increased peak intensity at *ca.* 250 nm suggests the formation of GSSG during irradiation.[42]

5′-GMP is a frequently used model for DNA binding of Pt drugs. After 1 h irradiation with blue light in the presence of 2 mol. equiv. of 5′-GMP (463 nm), $\{Pt^{II}(\mathbf{L2})_2(CH_3CN)(5'\text{-GMP-H})\}^+$ (peak b1, *m*/*z* 852, Fig. S28†), $\{Pt^{II}(\mathbf{L2})_2(N_3)(5'\text{-GMP})\}^+$ (b2, *m*/*z* 854), and $\{Pt^{II}(\mathbf{L2})_2(HCOO)(5'\text{-GMP})\}^+$ (b3, *m*/*z* 857) were detected as Pt-GMP adducts for **2**, while for **1**, only $\{a1, Pt^{II}(\mathbf{L1})_2(N_3)(5'\text{-GMP})\}^+$ (*m*/*z* 848) was observed by LC-MS (Fig. S28†). In both cases, *ca.* 63% of the 5′-GMP reacted.

Analysis of 2 in cell culture medium

To investigate the relationship between photoactivation of complex **2** and its photocytotoxicity, cell culture medium containing **2** (20 μM) after incubation with SW780 cells for 2 h in the dark or 1 h in the dark then 1 h irradiation (465 nm or 520 nm) was collected. Acetonitrile was added to precipitate proteins in this cell culture medium and the supernatant was analysed by LC-MS (Fig. S29†). Under normoxia, 62% and 10% of **2** underwent photodecomposition compared with the dark sample when irradiated with blue and green light, respectively. However, photoproducts were not detectable in this solution, which might be due to precipitation of these species or their binding to proteins and the detection limit of LC-MS. A similar decrease for blue light (65%) in the peak assigned to **2** was detected under hypoxia as in normoxia. In contrast, the decrease observed with green light was lower (42%).

Cellular accumulation and distribution

The cellular Pt accumulation for **2** (10 μM) was investigated in human A2780 and cisplatin resistant A2780cis ovarian cancer cells (Table S13†). Enhancements of 3.0 and 5.5× in Pt accumulation were observed for A2780 and A2780cis cells, respectively, treated with **2** upon irradiation (465 nm). Although the Pt accumulation after irradiation is similar in A2780 and A2780cis (3.3 and 3.8 ng per 10^6 cells) when treated with **2** at the same concentration (10 μM), the 2 h dark Pt accumulation of **2** is *ca.* 1.5× higher in A2780 than A2780cis, which matches well with the low dark cytotoxicity of **2**, and its ability to overcome cisplatin resistance.

The effect of oxygen concentration on the Pt accumulation was also studied for SW780 bladder cancer cells (Table S13† and Fig. 4b). In the dark, no apparent difference was observed in Pt accumulation for SW780 cells treated with **2** (10 μM) under normoxia and hypoxia. However, upon irradiation (465 nm), a significantly enhanced Pt accumulation (159×) was determined under hypoxia, while the enhancement under normoxia (5.5×) was relatively lower. The results indicate that the high photo-induced Pt accumulation under hypoxia might contribute to the hypoxia-enhanced photo-potency.

The cellular Pt distribution of **2** (10 μM) in SW780 cells after 2 h incubation in the dark was investigated under normoxia and hypoxia (Table S14† and Fig. 4c). Under normoxia, 51.4 ± 4.1%, 11.6 ± 0.9% and 37.0 ± 3.2% of Pt was located in nuclei, mitochondria and the cytoplasm, respectively. Notably, an increased Pt percentage in nuclei (67.2 ± 9.5%) was observed for **2** under hypoxia, which might contribute to its higher photocytotoxicity under hypoxia.

Mechanism of death

Apoptosis has long been recognised as the primary mechanism of cancer cell death induced by cisplatin and other platinum drugs, which is accompanied with cell shrinkage and membrane fragmentation.[43,44] Dual staining with Annexin V-FITC and PI was used to characterise the apoptosis induced in SW780 cells treated with **2**. After 1 h incubation, 1 h irradiation (465 nm) and 72 h further incubation with 20 μM under normoxia, 8.11% and 45.82% SW780 cells undergo early and late-stage apoptosis, respectively (Fig. 5). While in its dark control, only 1.49% and 6.67% cells are at early and late-stage apoptosis, respectively, which is similar to the dark cells that were not treated with **2**. Interestingly, when treated with 10 μM

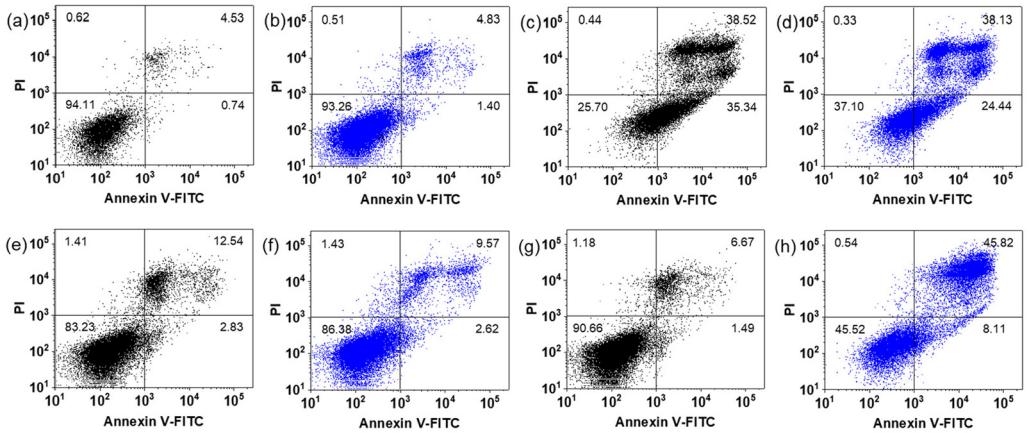

Fig. 5 Cell apoptosis assay for SW780 cells under normoxia double stained by Annexin V-FITC/PI ($\lambda_{ex}/\lambda_{em}$ = 488/500–560 nm for Annexin V-FITC, $\lambda_{ex}/\lambda_{em}$ = 488/645–735 nm for PI) and analysed by flow cytometry. (a) untreated SW780 cells in the dark; (b) untreated SW780 cells irradiated with blue light (465 nm); (c) SW780 cells treated with cisplatin (10 μM) in the dark and (d) irradiated with blue light; (e) SW780 cells treated with **2** (10 μM) in the dark and (f) irradiated with blue light; (g) SW780 cells treated with **2** (20 μM) in the dark and (h) irradiated with blue light. Percentages of cells in each status are shown.

2, 2.62% and 9.57% cells were at early and late-stage apoptosis, respectively, after irradiation, which is similar to those kept in the dark. Light alone did not contribute to apoptotic cell death. For comparison, cisplatin induced 35.34% early and 38.52% late-stage apoptosis in the dark, and irradiation did not enhance the apoptosis.

Different from normoxia, the level of apoptosis induced under hypoxia was much less (Fig. S30†). The percentage of SW780 cells at early-stage apoptosis increased from 0.38% to 1.55% and from 0.59% to 4.72% upon irradiation when treated with 10 and 20 μM **2**, respectively. The percentage of cells at late-stage apoptosis remained less than 1%. Additionally, cells treated with cisplatin showed no sign of apoptosis under hypoxia with an apoptosis proportion similar to untreated control (all <1%).

Ferroptosis is a programmed cell death mechanism, which is characterised by iron accumulation and lipid peroxidation.[45–47] BODYPI™ 581/591 C11 (5 μM, $\lambda_{ex}/\lambda_{em}$ = 488/500–560 nm) is a lipid peroxidation sensor that displays an emission maximum at 510 nm when oxidised. A significant emission increase at 500–560 nm was observed for SW780 cells treated with 10 μM **2** and irradiation (465 nm, 1 h) under normoxia when excited with 488 nm light (Fig. S31a†). Complex and light alone induced relatively little significant change in the emission. In contrast, no apparent change was detected when cells were treated with **2** and irradiation under hypoxia (Fig. S31b†). However, no apparent GSH level decrease was detected for SW780 cells treated with **2** and blue light. Thus, ferroptosis is not the main mechanism of cell death for **2** despite its ability to induce lipid peroxidation upon irradiation.

ROS generation

Excess levels of short-lived and highly reactive ROS cause cell damage to DNA, protein and lipids, which leads to activation of cell death processes.[48,49] Photoinduced ROS are important species for the photocytotoxicity of photoactived diazido Pt(IV) complexes.[26,50] SW780 cells were incubated with 10 μM **2** for 1 h, followed by 1 h irradiation (465 nm) and stained using DCFH-DA (20 μM, $\lambda_{ex}/\lambda_{em}$ = 488/501–627 nm) for 30 min (Fig. S32a†). Under normoxia, the irradiated cells display intense green emission, indicative of a large amount of ROS generation. The emission was quenched in the presence of 10 mM NAC (*N*-acetyl-L-cysteine), a ROS quencher. In contrast, cells treated without **2** or light show no apparent emission. Notably, no emission was observed in cells under hypoxia, even when treated with irradiated **2** (Fig. S32b†). These results suggest that ROS generation is not the main reason for induced cell death under hypoxia, which matches well with the conclusion that ferroptosis is not the main mechanism for **2** under hypoxia.

Mitochondrial membrane potential

The mitochondrial membrane potential is an important indicator of mitochondrial activity.[51] TMRE (tetramethylrhodamine ethyl ester) is a cell-permeant, cationic, red-orange fluorescent dye that accumulates in active mitochondria due to their relative negative charge. SW780 cells were incubated with 10 and 20 μM **2** for 1 h and irradiated (465 nm) for 1 h, with 0, 24 or 72 h further incubation under normoxia and hypoxia, then stained with TMRE (200 nM, $\lambda_{ex}/\lambda_{em}$ = 561/570–600 nm) for 30 min and analysed by flow cytometry (Fig. S33–35†). No apparent change was observed in cells immediately after irradiation under all conditions, except for cells treated with 20 μM **2** and irradiation (465 nm) under normoxia, in which some cells fail to sequester TMRE, indicating their decreased membrane potential (Fig. S33†). With 24 h further incubation, cells treated with **2** at 10 and 20 μM and irradiated lost their ability to uptake TMRE partially and completely under normoxia, respectively (Fig. S34†). In contrast, cells under hypoxia

exhibited reduced emission partially with 10 and 20 μM **2** after irradiation, but the decrease was more significant at the higher concentration. Notably, when the further incubation time was increased to 72 h, 20 μM **2** and irradiation induced dysfunctions of mitochondria in the majority of SW780 cells under both normoxia and hypoxia, while mitochondrial membrane potential changes induced by 10 μM irradiated **2** were only observed under hypoxia, the flow cytometry data under normoxia show little difference from the dark control (Fig. S35†). Light alone and complex in the dark can cause no apparent change in mitochondrial activity.

To confirm the results obtained from flow cytometry, confocal microscopy was also used to investigate the TMRE accumulation in SW780 cells incubated with **2** for 1 h and irradiated (465 nm) for 1 h, with 72 h further incubation, and stained with TMRE (200 nM, $\lambda_{ex}/\lambda_{em}$ = 561/566–685 nm, Fig. 6). In cells treated with light or complex alone, TMRE localised in mitochondria and exhibited yellow emission under both normoxia and hypoxia. However, under hypoxia, cells treated with irradiated **2** at different concentrations (5, 10 and 20 μM) showed no TMRE emission, indicating the dysfunction of mitochondria. In contrast, only cells treated with irradiated 20 μM **2** showed no TMRE emission under normoxia. Cells treated with 5 and 10 μM **2** were still able to take up TMRE into mitochondria, although apparent swelling was observed for cells treated at 10 μM. These results match well with those from flow cytometry.

Liver microsomal stability

Liver microsomal stability is an important property for early-stage drug candidates.[52] Metabolic stability *in vivo* is particularly essential for photoactive agents to ensure they can arrive intact at target sites. Complex **2** (100 μM) was incubated with liver microsomes and NADPH at 310 K in the dark for 24 h in both air- and N_2-saturated PBS solution for 24 h (Fig. S36†). Complex **2** exhibited high stability towards liver microsomes in the presence of oxygen, while 46% of **2** underwent decomposition in N_2-saturated solution, indicating that a more reductive environment can accelerate the reduction of Pt(IV) or nitroimidazole. However, no reduction products were detectable due to the relatively low sensitivity of LC-MS.

Accumulation in rat bladder

Intravesical instillation is a frequently used administration method for bladder cancer drugs.[53] Therefore, drug accumulation in bladder before and after irradiation plays an important role in the efficacy of photoactive Pt anticancer drugs. Fresh bladders from female Sprague–Dawley® rats were cut and flattened, then incubated with 50 μM complex **2** in PBS in the dark for 1 h at 310 K. One bladder was irradiated with blue light (465 nm) for 1 h, while the other one was kept in the dark. Slightly less Pt appeared to accumulate in the bladder kept in the dark compared to the irradiated bladder (6.2 ± 1.0 *versus* 9.5 ± 1.4 ng Pt mg^{-1}, respectively, Table S15†).

Discussion

BC is the costliest cancer for treatment. It was the first cancer approved to be treated by PDT, and new phototherapeutic agents with ability to overcome hypoxia resistance and suitable activation wavelengths to control the depth of light penetration are under development.[9,20] The strongly electron-withdrawing nitro group can be activated by reduction under hypoxia and Pt-nitroimidazole complexes have been investigated as hypoxia-sensitive radiosensitisers.[37–40] Photoactive Pt(IV) complexes with nitroimidazole ligands have not been reported before. In this work, we prepared a series of novel photoactive diazido Pt(IV) complexes with varied substituents on the equatorial ligands. Among them, complex **2** with nitroimidazole ligands exhibit enhanced photocytotoxicity under hypoxia, especially with green light exposure. Its photochemical, photobiological and *ex vivo* properties were investigated to explore the potential mechanism of action.

Synthesis and X-ray structures

Photoactive diazido Pt(IV) complexes **1–6** were synthesised and characterised. All complexes gave satisfactory NMR, HR-MS

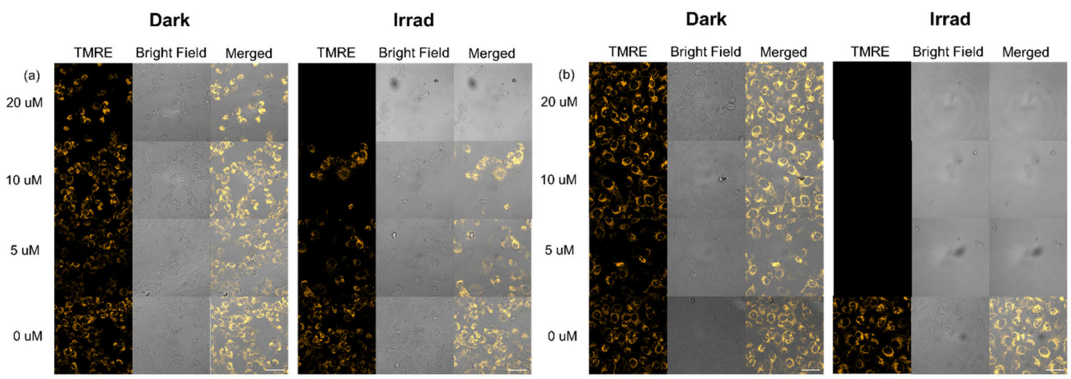

Fig. 6 Confocal fluorescence microscopy images of mitochondrial membrane potential changes for SW780 cells treated with **2** (0, 5, 10 and 20 μM) in the dark (74 h), or 1 h incubation and 1 h irradiation (465 n) and 72 h further incubation without drug removal, then stained by TMRE ($\lambda_{ex}/\lambda_{em}$ = 561/566–685 nm) under (a) normoxia and (b) hypoxia. Scale bar = 50 μm.

and HPLC purity. Among them, complex **3** was purified by semi-preparative HPLC, and **2**, **4** and **5** by Biotage with a Biotage® Sfär C18 D column chromatography due to by-products with similar R_f values on TLC, while **1** and **6** were purified by column chromatography on silica gel. An all *trans* configuration was observed for both complexes and their octahedral platinum centre with an $[N_4O_2]$ geometry is similar to **FM190**. Notably, the two imidazole ligands in **2** do not lie in the same plane, probably due to packing effects, while **1** and **3–6** exhibit a symmetric structure.

Absorption spectra, photoactivation and photocytotoxicity

Similar to **FM190**, an absorption maximum at *ca.* 290 nm was detectable for all complexes, and assigned to LMCT from azide to Pt(IV). The presence of the various substituents in the pyridine ligands do not result in significant spectral changes in the corresponding complexes, except for methoxy in **4**, which is responsible for the absorbance at 242 nm with a high extinction coefficient. In contrast, the absorbance ascribed to nitroimidazole in **2** overlaps with the LMCT band, so the extinction coefficient of peak at 289 nm is much higher than that of **FM190**. Due to their similar absorption spectra, photoactivation of these complexes with blue and green light irradiation monitored by UV-vis exhibited no apparent differences. Although no apparent absorption band in the range 400–600 nm can be detected for these complexes, their photoactivation using blue and green lights is achievable. The reason for this might be that absorption bands in this region are weak and broad.[30]

However, their photocytotoxicity towards SW780 bladder cancer cells is significantly affected by the amine substituents. Complexes with strong electron-withdrawing substituents exhibit higher photocytotoxicity than **FM190** and enhanced photocytotoxicity under hypoxia than normoxia, especially with green light. This might be due to the ability of the electron-withdrawing substituents to reduce the stability of the Pt(IV) complexes, thus enhancing their photoreduction, especially under a reductive environment with low oxygen concentration. However, complexes **1** and **6** also showed high dark cytotoxicity, but the dark cytotoxicity of **2** is low. Thus, **2** was selected as the lead compound for further investigation, and **1** was also studied to compare the effect of imidazole and pyridine ligands.

Photochemistry and photocytotoxicity of complexes 1 and 2 with nitro substituents

High dark stability was observed for both complexes **1** ($3NO_2Py$) and **2** ($4Me5NO_2Im$) with nitro substituents in aqueous solution, even in the presence of bioreductants, under both normoxia and hypoxia. They generate Pt(II) and Pt(IV) species, as well as azidyl radicals and singlet oxygen upon irradiation. However, these two compounds exhibit different photoactivation modes, with release of **L1** ligand detected for **1**, while no **L2** was detected for **2** after irradiation. The photoactivation rate in the presence of GSH under hypoxia is faster than that under normoxia, which might be due to the more reductive environment and matches well with the enhanced photocytotoxicity under hypoxia. The number of Pt-GMP species detected for **2** is higher than for **1**, suggesting a potentially more complicated DNA binding mode in cells.

Complex **2** exhibits no apparent dark cytotoxicity towards all cell lines studied under both normoxia and hypoxia, while moderate dark cytotoxicity was determined for **1**. This matches well with the more negative reduction potential of **2**, indicating its higher dark stability. Upon irradiation, both compounds exhibit significantly enhanced photocytotoxicity. The higher extent of photodecomposition for **2** under blue light than green light matches well with the higher photocytotoxicity detected with blue light under normoxia. Notably, with green light irradiation, these complexes show much higher photocytotoxicity under hypoxia. This result can be explained by the extent of photoactivation of **2** in cell culture medium under hypoxia, which is much higher (4×) than that with green light under normoxia. In addition, these complexes display significant ability to overcome cisplatin resistance, owing to their different mechanism of action compared with cisplatin and traditional Pt drugs. The low cytotoxicity towards normal cells is also noticeable. Since ROS generation is an important mechanism for these complexes, the lower ROS level in normal cells might allow them to tolerate increased ROS during treatment.[49]

Cellular accumulation and mechanism of action of 2

The cellular Pt accumulation and mechanism studies on SW780 bladder cancer cells were investigated for lead compound **2**. The improved photocytotoxicity of **2** may be due to the enhanced cellular accumulation of Pt; Pt(II) photoproducts exhibit higher reactivity and are readily bound within cells, so reducing efflux. Notably, under hypoxia, higher nucleus Pt distribution in the dark combined with the enhanced photoactivation in the reductive environment under hypoxia are likely to contribute to the overall high photocytotoxicity of **2** under hypoxia.

Apoptosis was detected as a mechanism of cell death after irradiation of **2** under normoxia, while only mild apoptosis was observed under hypoxia. Also, photoinduced lipid peroxidation and ROS generation can be seen only under normoxia. However, irradiation of **2** can cause mitochondrial membrane potential changes more significantly at low concentration under hypoxia. The photoinduced Pt accumulation is also much higher under hypoxia. These results suggest that the mechanism of action for **2** is different under normoxia and hypoxia.

Ex vivo studies of 2

High liver microsomal stability was observed for **2** in the dark in air-saturated solution, while *ca.* 50% of **2** decomposed in N_2-saturated solutions. These results match well with the higher reduction tendency of nitroimidazole and Pt(IV) complexes under reductive environments. However, the reduced products were not detectable, thus the detailed mechanism

will need to be further explored. Similar to the *in vitro* results, irradiation can enhance Pt accumulation in rat bladder treated with **2**. As a result, light-directed activation and accumulation of **2** within bladder can be achieved to improve the selectivity for tumour over healthy tissue.

Conclusions

A series of six novel photoactive diazido Pt(IV) complexes with varied *N*-heterocyclic amine ligands was synthesised and structurally characterised by X-ray crystallography. Their photoactivation and photocytotoxicity towards bladder cancer cells were screened, resulting in the selection of lead complex **2** (*trans*, *trans*, *trans*-$[Pt(N_3)_2(OH)_2(1\text{-methyl-5-nitroimidazole})_2]$) with *trans* nitroimidazole ligands that exhibits promising photocytotoxicity towards bladder cancer cells under both normoxia and hypoxia. The irreversible reduction wave assigned to Pt^{IV}/Pt^{II} follows the trend that the reduction potential for **2** is more negative than **FM190** and its nitropyridine analogue **1**, matching the trend of their dark cytotoxicity.

Complex **2** exhibited high dark stability and photoactivation with visible light in air- or N_2-saturated aqueous solutions. Azidyl radicals, singlet oxygen and Pt-GMP adducts were detected upon irradiation. Complex **2** exhibited no apparent dark cytotoxicity towards all cell lines under both normoxia and hypoxia. Promising photocytotoxicity towards various cancer cell lines under varied oxygen concentrations was observed for this complex with visible light, but its photocytotoxicity towards normal bladder cells is at least 3× lower than that to bladder cancer cells. Notably, green light photocytotoxicity was significantly enhanced under hypoxia than normoxia, which matches well with the higher extent of its photoreduction in cell culture media under hypoxia. The ability to circumvent cisplatin resistance was observed for **2**, which exhibited enhanced cellular Pt accumulation upon irradiation, especially under hypoxia. Photoinduced ROS generation, apoptosis and lipid peroxidation were observed for **2** under normoxia, but not under hypoxia. In contrast, higher nuclear Pt accumulation and more apparent photoinduced mitochondrial membrane potential changes were observed under hypoxia. In addition, **2** exhibited high liver microsomal dark stability and photo-enhanced Pt accumulation in rat bladder, which suggests its potential to be used as phototherapeutic agent in the clinics for BC treatment. Having selected complex **2** as a candidate for further preclinical development, the next steps will involve further toxicology and *in vivo* screening in appropriate bladder cancer models.

Author contributions

HS designed the project and carried out experiments; PJS supervised the research; GJC carried out X-ray crystallography. HS and PJS analysed and interpreted the results and drafted the script. All authors contributed to the final submission.

Data availability

The data supporting this article have been included as part of the ESI.†

Conflicts of interest

There are no conflicts to declare.

Acknowledgements

We thank the Engineering and Physical Sciences Research Council (EPSRC grant no. EP/P030572/1) and Anglo-American Platinum for funding. We thank Dr Richard T. Bryan (University of Birmingham) for providing SW-780 and VM-CUB-1 bladder cancer cells, Professor Elizabeth Wellington (University of Warwick) for access to the hypoxic chamber and BSU team at University of Warwick for providing rat bladders. Single-crystal X-ray diffraction measurements were made using equipment housed within the X-ray Diffraction Research Technology Platform at Warwick with funding from EPSRC grant EP/X034836/1. We thank Professor Peter A. Charlton (University of Warwick) for helpful discussion of cell data.

References

1 H. Shi and P. J. Sadler, How promising is phototherapy for cancer?, *Br. J. Cancer*, 2020, **123**, 871–873.
2 W. Jiang, M. Liang, Q. Lei, G. Li and S. Wu, The current status of photodynamic therapy in cancer treatment, *Cancers*, 2023, **15**, 585.
3 G. Gunaydin, M. E. Gedik and S. Ayan, Photodynamic therapy for the treatment and diagnosis of cancer–a review of the current clinical status, *Front. Chem.*, 2021, **9**, 686303.
4 H. Shi, C. Imberti and P. J. Sadler, Diazido platinum(IV) complexes for photoactivated anticancer chemotherapy, *Inorg. Chem. Front.*, 2019, **6**, 1623–1638.
5 H. Shi and P. J. Sadler, Advances in the design of photoactivated platinum anticancer complexes, *Adv. Inorg. Chem.*, 2022, **80**, 95–127.
6 H. Shi and P. J. Sadler, Photoactive metallodrugs, in *Compr. Inorg. Chem. III*, 2023, pp. 507–552.
7 X. Jing, F. Yang, C. Shao, K. Wei, M. Xie, H. Shen and Y. Shu, Role of hypoxia in cancer therapy by regulating the tumor microenvironment, *Mol. Cancer*, 2019, **18**, 157.
8 B. Muz, P. de la Puente, F. Azab and A. K. Azab, The role of hypoxia in cancer progression, angiogenesis, metastasis, and resistance to therapy, *Hypoxia*, 2015, **3**, 83–92.
9 R. S. Svatek, B. K. Hollenbeck, S. Holmäng, R. Lee, S. P. Kim, A. Stenzl and Y. Lotan, The economics of bladder cancer: costs and considerations of caring for this disease, *Eur. Urol.*, 2014, **66**, 253–262.
10 J. Y. C. Teoh, A. M. Kamat, P. C. Black, P. Grivas, S. F. Shariat and M. Babjuk, Recurrence mechanisms of

non-muscle-invasive bladder cancer - a clinical perspective, *Nat. Rev. Urol.*, 2022, **19**, 280–294.

11 L. M. C. van Hoogstraten, A. Vrieling, A. G. van der Heijden, M. Kogevinas, A. Richters and L. A. Kiemeney, Global trends in the epidemiology of bladder cancer: challenges for public health and clinical practice, *Nat. Rev. Clin. Oncol.*, 2023, **20**, 287–304.

12 R. J. Jones, S. J. Crabb, M. Linch, A. J. Birtle, J. McGrane, D. Enting, R. Stevenson, K. Liu, B. Kularatne and S. A. Hussain, Systemic anticancer therapy for urothelial carcinoma: UK oncologists' perspective, *Br. J. Cancer*, 2024, **130**, 897–907.

13 F. Li, Z. Zheng, W. Chen, D. Li, H. Zhang, Y. Zhu, Q. Mo, X. Zhao, Q. Fan, F. Deng, C. Han and W. Tan, Regulation of cisplatin resistance in bladder cancer by epigenetic mechanisms, *Drug Resistance Updates*, 2023, **68**, 100938.

14 S. Liu, X. Chen and T. Lin, Emerging strategies for the improvement of chemotherapy in bladder cancer: Current knowledge and future perspectives, *J. Adv. Res.*, 2022, **39**, 187–202.

15 K. Ding, L. Wang, J. Zhu, D. He, Y. Huang, W. Zhang, Z. Wang, A. Qin, J. Hou and B. Z. Tang, Photo-enhanced chemotherapy performance in bladder cancer treatment via albumin coated AIE aggregates, *ACS Nano*, 2022, **16**, 7535–7546.

16 H. Li, G. Long and J. Tian, Efficacy and safety of photodynamic therapy for non–muscle-invasive bladder cancer: a systematic review and meta-analysis, *Front. Oncol.*, 2023, **13**, 1255632.

17 Y. Chen, L. Gu, B. Ma, X. Li, Y. Mei, J. Zhou, Y. Chong, M. Ma, M. Zhang, L. Wang, Y. Cheng, K. Wu, J. Zeng, M. Cheng, P. Guo, P. Zhang and D. He, Photoactivatable metal organic framework for synergistic ferroptosis and photodynamic therapy using 450 nm laser, *Chem. Eng. J.*, 2023, **454**, 140438.

18 S. Monro, K. L. Colón, H. Yin, J. Roque, P. Konda, S. Gujar, R. P. Thummel, L. Lilge, C. G. Cameron and S. A. McFarland, Transition metal complexes and photodynamic therapy from a tumor-centered approach: challenges, opportunities, and highlights from the development of TLD1433, *Chem. Rev.*, 2019, **119**, 797–828.

19 H. Fukushima, S. Takao, A. Furusawa, V. Valera Romero, S. Gurram, T. Kato, S. Okuyama, M. Kano, P. L. Choyke and H. Kobayashi, Near-infrared photoimmunotherapy targeting Nectin-4 in a preclinical model of bladder cancer, *Cancer Lett.*, 2024, **585**, 216606.

20 M. R. Hamblin, Photodynamic therapy for cancer: what's past is prologue, *Photochem. Photobiol.*, 2020, **96**, 506–516.

21 K. M. M. Rahman, P. Giram, B. A. Foster and Y. You, Photodynamic therapy for bladder cancers, a focused review, *Photochem. Photobiol.*, 2023, **99**, 420–436.

22 E. H. Streeter and A. L. Harris, Angiogenesis in bladder cancer-prognostic marker and target for future therapy, *Surg. Oncol.*, 2002, **11**, 85–100.

23 A. F. Westendorf, J. A. Woods, K. Korpis, N. J. Farrer, L. Salassa, K. Robinson, V. Appleyard, K. Murray, R. Grünert, A. M. Thompson, P. J. Sadler and P. J. Bednarski, *Trans*,*trans*,*trans*-[PtIV(N_3)$_2$(OH)$_2$(py)(NH_3)]: A light-activated antitumor platinum complex that kills human cancer cells by an apoptosis-independent mechanism, *Mol. Cancer Ther.*, 2012, **11**, 1894–1904.

24 P. J. Bednarski, R. Grünert, M. Zielzki, A. Wellner, F. S. Mackay and P. J. Sadler, Light-activated destruction of cancer cell nuclei by platinum diazide complexes, *Chem. Biol.*, 2006, **13**, 61–67.

25 N. J. Farrer, J. A. Woods, L. Salassa, Y. Zhao, K. S. Robinson, G. Clarkson, F. S. MacKay and P. J. Sadler, A potent *trans*-diimine platinum anticancer complex photoactivated by visible light, *Angew. Chem., Int. Ed.*, 2010, **49**, 8905–8908.

26 H. Shi, F. Ponte, J. S. Grewal, G. J. Clarkson, C. Imberti, I. Hands-Portman, R. Dallmann, E. Sicilia and P. J. Sadler, Tuning the photoactivated anticancer activity of Pt(iv) compounds via distant ferrocene conjugation, *Chem. Sci.*, 2024, **15**, 4121–4134.

27 E. Shaili, L. Salassa, J. A. Woods, G. Clarkson, P. J. Sadler and N. J. Farrer, Platinum(IV) dihydroxido diazido *N*-(heterocyclic)imine complexes are potently photocytotoxic when irradiated with visible light, *Chem. Sci.*, 2019, **10**, 8610–8617.

28 F. S. Mackay, J. A. Woods, P. Heringova, J. Kašpárková, A. M. Pizarro, S. A. Moggach, S. Parsons, V. Brabec and P. J. Sadler, A potent cytotoxic photoactivated platinum complex, *Proc. Natl. Acad. Sci. U. S. A.*, 2007, **104**, 20743–20748.

29 S. Noriega, J. Cardoso-Ortiz, A. López-Luna, M. D. R. Cuevas-Flores and J. A. Flores De La Torre, The diverse biological activity of recently synthesized nitro compounds, *Pharmaceuticals*, 2022, **15**, 717.

30 H. C. Tai, Y. Zhao, N. J. Farrer, A. E. Anastasi, G. Clarkson, P. J. Sadler and R. J. Deeth, A computational approach to tuning the photochemistry of platinum(IV) anticancer agents, *Chem. – Eur. J.*, 2012, **18**, 10630–10642.

31 O. P. S. Patel, O. J. Jesumoroti, L. J. Legoabe and R. M. Beteck, Metronidazole-conjugates: a comprehensive review of recent developments towards synthesis and medicinal perspective, *Eur. J. Med. Chem.*, 2021, **210**, 112994.

32 P. J. Jenks, Nitroimidazoles: metronidazole, ornidazole and tinidazole, *Infect. Dis.*, 2010, 1413–1414.

33 J. Müller, A. Hemphill and N. Müller, Physiological aspects of nitro drug resistance in Giardia lamblia, *Int. J. Parasitol.: Drugs Drug Resist.*, 2018, **8**, 271–277.

34 R. Czarnomysy, D. Radomska, A. Muszynska, J. M. Hermanowicz, I. Prokop, A. Bielawska and K. Bielawski, Evaluation of the anticancer activities of novel transition metal complexes with berenil and nitroimidazole, *Molecules*, 2020, **25**, 2860.

35 R. Navarro-Peñaloza, B. Landeros-Rivera, H. López-Sandoval, R. Castro-Ramírez and N. Barba-Behrens, New insights on transition metal coordination compounds with biological active azole and nitroimidazole derivatives, *Coord. Chem. Rev.*, 2023, **494**, 215360.

36 G. E. Giacomazzo, L. Conti, C. Fagorzi, M. Pagliai, C. Andreini, A. Guerri, B. Perito, A. Mengoni, B. Valtancoli and C. Giorgi, Ruthenium(II) polypyridyl complexes and metronidazole derivatives: a powerful combination in the design of photoresponsive antibacterial agents effective under hypoxic conditions, *Inorg. Chem.*, 2023, **62**, 7716–7727.

37 F. M. Macdonald and P. J. Sadler, Multinuclear MR studies of platinum(II) nitroimidazole complexes: ^{15}N-labelling and reactions with nucleotides, *Magn. Reson. Chem.*, 1991, **29**, S52–S59.

38 K. A. Skov, H. Adomat, D. J. Chaplin and N. P. Farrell, Toxicity of $[PtCl_2(NH_3)L]$ in hypoxia; L = misonidazole or metronidazole, *Anticancer Drug Des.*, 1990, **5**, 121–128.

39 J. R. Bales, P. J. Sadler, C. J. Coulson, M. Laverick and A. H. W. Nias, Hypoxic cell sensitization to radiation damage by a new radiosensitizer: cis-dichloro-bis(1-(2-hydroxyethyl)-2-methyl-5-nitroimidazole-N^3)platinum(II) (flap), *Br. J. Cancer*, 1982, **46**, 701–705.

40 F. D. Rochon, P. Kong, R. Melanson and K. A. Skov, Characterization and properties of monoammine nitroimidazole complexes of platinum $[PtCl_2(NH_3)(NO_2Im)]$. Crystal and molecular structure of c/s-amminedichloro(l-{(((2-hydroxyethyl)amino)carbonyl)methyl}-2-nitroimidazole) platinum(II), *Inorg. Chem.*, 1991, **30**, 4531–4535.

41 J. S. Butler, J. A. Woods, N. J. Farrer, M. E. Newton and P. J. Sadler, Tryptophan switch for a photoactivated platinum anticancer complex, *J. Am. Chem. Soc.*, 2012, **134**, 16508–16511.

42 Z. Abedinzadeh, M. Gardes-Albert and C. Ferradini, Kinetic study of the oxidation mechanism of glutathione by hydrogen peroxide in neutral aqueous medium, *Can. J. Chem.*, 1989, **67**, 1247–1255.

43 S. Ghosh, Cisplatin: the first metal based anticancer drug, *Bioorg. Chem.*, 2019, **88**, 102925.

44 G. Coffetti, M. Moraschi, G. Facchetti and I. Rimoldi, The challenging treatment of cisplatin-resistant tumors: state of the art and future perspectives, *Molecules*, 2023, **28**, 3407.

45 S. Sun, J. Shen, J. Jiang, F. Wang and J. Min, Targeting ferroptosis opens new avenues for the development of novel therapeutics, *Signal Transduction Targeted Ther.*, 2023, **8**, 372.

46 Y. Wang, X. Wu, Z. Ren, Y. Li, W. Zou, J. Chen and H. Wang, Overcoming cancer chemotherapy resistance by the induction of ferroptosis, *Drug Resistance Updates*, 2023, **66**, 100916.

47 D. Coradduzza, A. Congiargiu, Z. Chen, A. Zinellu, C. Carru and S. Medici, Ferroptosis and senescence: a systematic review, *Int. J. Mol. Sci.*, 2023, **24**, 3658.

48 R. Wang, L. Liang, M. Matsumoto, K. Iwata, A. Umemura and F. He, Reactive Oxygen Species and NRF_2 Signaling, Friends or Foes in Cancer?, *Biomolecules*, 2023, **13**, 353.

49 H. Zhang, Z. Mao, Y. Kang, W. Zhang, L. Mei and X. Ji, Redox regulation and its emerging roles in cancer treatment, *Coord. Chem. Rev.*, 2023, **475**, 214897.

50 H. Shi, C. Imberti, G. J. Clarkson and P. J. Sadler, Axial functionalisation of photoactive diazido platinum(iv) anticancer complexes, *Inorg. Chem. Front.*, 2020, **7**, 3533–3540.

51 S. Mukherjee, G. K. Bhatti, R. Chhabra, P. H. Reddy and J. S. Bhatti, Targeting mitochondria as a potential therapeutic strategy against chemoresistance in cancer, *Biomed. Pharmacother.*, 2023, **160**, 114398.

52 S. N. R. Gajula, N. Nadimpalli and R. Sonti, Drug metabolic stability in early drug discovery to develop potential lead compounds, *Drug Metab. Rev.*, 2021, **53**, 459–477.

53 M. T. Melgarejo-Segura, A. Morales-Martínez, Y. Yáñez-Castillo, M. Á. Arrabal-Polo, P. Gómez-Lechuga, M. Pareja-Vílchez, J. J. Jiménez-Moleón and M. A. Martín, A systematic review of the efficacy of intravesical electromotive drug administration therapy for non-muscle invasive bladder cancer, *Urol. Oncol.: Semin. Orig. Invest.*, 2023, **41**, 166–176.